

# JGR Space Physics

## RESEARCH ARTICLE

10.1029/2022JA030473

### Key Points:

- Two Pc5 wave events we analyzed were highly dawn-dusk asymmetric, with stronger magnetic field perturbations on the dawnside than duskside
- Slow or drift mirror mode waves coupled with standing Alfvén waves in the magnetosphere were driven by the magnetopause surface waves
- Surface waves by Kelvin-Helmholtz instability along the magnetopause is suggested to be the source of the dawnside Pc5 waves

### Supporting Information:

Supporting Information may be found in the online version of this article.

### Correspondence to:

W. Zhang,  
wzhang1@bu.edu

### Citation:

Zhang, W., Nishimura, Y., Wang, B., Hwang, K.-J., Hartinger, M. D., Donovan, E. F., et al. (2022). Identifying the structure and propagation of dawnside Pc5 ULF waves using space-ground conjunctions. *Journal of Geophysical Research: Space Physics*, 127, e2022JA030473. <https://doi.org/10.1029/2022JA030473>

Received 17 MAR 2022  
Accepted 8 DEC 2022

## Identifying the Structure and Propagation of Dawnside Pc5 ULF Waves Using Space-Ground Conjunctions

W. Zhang<sup>1</sup> , Y. Nishimura<sup>1</sup> , B. Wang<sup>2</sup> , K.-J. Hwang<sup>3,4</sup> , M. D. Hartinger<sup>5</sup> , E. F. Donovan<sup>6</sup> , V. Angelopoulos<sup>7</sup> , and D. Hampton<sup>8</sup> 

<sup>1</sup>Department of Electrical and Computer Engineering and Center for Space Sciences, Boston University, Boston, MA, USA,

<sup>2</sup>Institute of Space Science and Applied Technology, Harbin Institute of Technology (Shenzhen), Shenzhen, China,

<sup>3</sup>NASA Goddard Space Flight Center, Greenbelt, MD, USA, <sup>4</sup>Goddard Planetary and Heliophysics Institute, University of Maryland, Baltimore County, Baltimore, MD, USA, <sup>5</sup>Space Science Institute, Boulder, CO, USA, <sup>6</sup>Department of Physics and Astronomy, University of Calgary, Calgary, AB, Canada, <sup>7</sup>Department of Earth, Planetary, and Space Sciences, University of California, Los Angeles, Los Angeles, CA, USA, <sup>8</sup>Geophysical Institute, University of Alaska Fairbanks, Fairbanks, AK, USA

**Abstract** Pc5 ultralow frequency waves are important for transferring energy between the magnetosphere and ionosphere. While many observations have been performed on Pc5 waves properties, it has been difficult to determine the source region, signal propagation path, and the two-dimensional structure of Pc5 waves beyond coverage by a small number of satellites. Pc5 waves often show a dawn-dusk asymmetry, but the cause of the asymmetry is under debate. To address these issues, we used conjunction events between the THEMIS satellites and all-sky imagers and analyzed two Pc5 wave events that were stronger on the dawnside. For both events, the Pc5 waves propagated from dawnside magnetopause toward the nightside magnetosphere. The Pc5 waves were also associated with dawnside magnetopause surface waves, which were probably induced by the Kelvin-Helmholtz instability. The ionospheric equivalent currents identified multiple vortices on the dawnside associated with quasi-periodic auroral arcs and much weaker perturbations on the duskside. Global auroral imaging also presented a similar dawn-dusk asymmetry with multiple arcs on the dawnside, while only one or two major arcs existed on the duskside. Pc5 waves in the magnetosphere had an anti-phase relation between the total magnetic field and thermal pressure, with a slower propagation velocity compared with magnetohydrodynamic waves. The Poynting flux was anti-sunward with an oscillating field-aligned component. These properties suggest that Pc5 waves were slow or drift mirror mode waves coupled with standing Alfvén waves. The ground-based and multi-satellite observations provide crucial information for determining the Pc5 waves properties, possible source region, and signal propagation path.

**Plain Language Summary** Pc5 ultralow frequency waves (1.66–6.66 mHz) are large-scale waves in space, and Pc5 waves are capable of interacting with particles and modulating higher frequency waves, resulting in energy transfer in the magnetosphere-ionosphere system. However, it is difficult to find the exact signal propagation path and identify the source due to the limited sparse satellite observations in space. We investigated two Pc5 wave events by using the conjunctions of ground magnetometers, all-sky imagers, and Time History of Events and Macroscale Interaction During Substorms (THEMIS) satellites. We found that the aurora shows periodic intensification and the ionospheric currents had multiple vortices with dawn-dusk asymmetry. The Pc5 waves in the magnetosphere are identified as standing waves that were coupled with surface waves at the magnetopause traveling anti-sunward. We suggest that magnetopause surface waves were induced by Kelvin-Helmholtz instability and drive the Pc5 waves. The dawn-dusk asymmetry of Kelvin-Helmholtz instability in the magnetosheath may explain the current asymmetric pattern in the ionosphere.

## 1. Introduction

Pc5 ultralow frequency (ULF) waves (frequency between 1.66 and 6.66 mHz, or period of 150–600 s) play a significant role in energy transfer in the magnetosphere-ionosphere system (Greenwald & Walker, 1980; Zong et al., 2017). ULF waves also modulate higher-frequency waves, for example, whistler-mode waves (Bell, 1976; W. Li et al., 2011; Nambu et al., 1986), that resonate with energetic particles (Elkington et al., 1999; Fei et al., 2006; Ren et al., 2016; Ren, Zong, Zhou, et al., 2017; Rostoker et al., 1998) and create diffuse aurora (Motoba

et al., 2021). ULF waves provide a useful diagnostic tool of several magnetospheric properties, such as particle scattering and precipitation (Engebretson et al., 2008; Liu et al., 1999), and ground phenomena, for example, the geomagnetically induced currents (GIC) may damage technological infrastructures (Pulkkinen et al., 2017; Yagova et al., 2021). Ground-based and space-based observations show that Pc5 events with low azimuthal wave numbers have global distribution over almost all magnetic local times (MLTs) (Liou & Takahashi, 2013; Shi et al., 2018), while events with larger wave numbers tend to be more localized (Hao et al., 2020; Sarris et al., 2009).

Pc5 waves are excited mainly due to external sources, which consist of solar wind variations, magnetosheath disturbances, and magnetopause oscillations including Kelvin-Helmholtz (KH) instability (Claudepierre et al., 2010; Kepko & Spence, 2003; Liu et al., 2009; Mann et al., 1999; Shen et al., 2018; Walker, 1981; Zong et al., 2017). The solar wind dynamic pressure modulations can directly drive Pc5 waves (Kepko et al., 2002; Vidal-Luengo & Moldwin, 2021; Zhang et al., 2010). Kelvin-Helmholtz (KH) instability on the flanks of the magnetopause can excite surface waves along the magnetopause (M. Archer et al., 2021; Chen & Hasegawa, 1974; Claudepierre et al., 2008; Pu & Kivelson, 1983). The surface waves along the magnetopause can be a source of global waveguide modes in the magnetosphere that couple to standing Alfvén waves through mode conversion (Fujita et al., 1996; Glassmeier et al., 1999). KH instability is traditionally considered to occur in the northward interplanetary magnetic field (IMF) and high solar wind speed condition, but it can also occur in various IMF polarities (H. Hasegawa et al., 2004; Kavosi & Raeder, 2015; Takahashi & Ukhorskiy, 2008).

The drift mirror instability is one of the internal generation mechanisms for Pc5 waves. The key features of drift mirror waves include an anti-phase relation between the total magnetic field and plasma density or pressure, high plasma beta ( $\beta$ ), and the presence of both cold and hot plasma (A. Hasegawa, 1969; Southwood, 1976). Drift mirror waves propagate much more slowly than magnetohydrodynamic (MHD) waves, and the propagation velocity can be used to distinguish the two wave modes. Observations suggest that the magnetic equator in the outer magnetosphere often satisfies the drift mirror instability threshold ( $\beta_{\perp}(P_{\perp}/P_{\parallel} - 1) > 1$ ) (A. Hasegawa, 1969; Soto-Chavez et al., 2019), and plasma beta is usually larger than 1 (Zhu & Kivelson, 1994).

Ionospheric equivalent currents from ground magnetometer networks describe two-dimensional structures of horizontal currents, assuming a uniform conductance and that the magnetic field variations primarily arise from Hall currents (Glassmeier, 1980; McHenry et al., 1990). By calculating the equivalent currents, Motoba et al. (2003) inferred that the ionospheric current perturbations generated by Pc5 waves formed two vortices on the dawnside and duskside. Later, simulation results supported the presence of the two-cell current pattern (Motoba et al., 2007). Their event had global Pc5 wave activity with substantial wave amplitudes in both dawn and dusk sectors. However, it is not understood what the equivalent current system is for Pc5 waves with large dawn-dusk asymmetric perturbations.

Pc5 waves on the ground may have a longitudinal dependence (L. Li et al., 2017), and often have a strong dawn-dusk asymmetry, with a preference on the dawnside (Baker et al., 2003; Gillies et al., 2018; Vernerstrøm, 1999). Observations of dawnside preference of Pc5 waves have been reported using satellite observations such as Ampe/CCE (Anderson et al., 1990), DE 1 (Nosé et al., 1995), Geotail (Kokubun, 2013) and THEMIS (Takahashi, Hartinger, et al., 2015). I. Rae et al. (2005) reported that Pc5 pulsations can also be stronger on the duskside, and they attributed this event to the field-line resonance and magnetospheric waveguide originating from magnetopause oscillations. Ren, Zong, Miyoshi, et al. (2017) reported one Pc5 oscillation on the duskside exited by the localized drift-bounce instability. Zhao et al. (2020) stated that the localized ULF waves trapped in the plume lead to a wave-electron interaction at noon-to-dusk region.

Although a number of studies on Pc5 ULF waves have been performed, it is often difficult to find the source of Pc5 waves, signal propagation path to the ionosphere, and the cause of the dawn-dusk asymmetry, mainly due to the limited number of measurement points by satellites and ground magnetometers. In this paper, we address these issues by using multi-point observations in the magnetosphere and magnetopause by the Time History of Events and Macroscale Interactions during Substorms (THEMIS) satellites together with ground magnetometers, ground-based and space-based auroral imaging. We analyzed two Pc5 wave events that were stronger on the dawnside and examined the driving source, wave propagation direction, and the ionospheric equivalent currents.

This paper is organized as follows. The data and methods are described in Section 2. Section 3 describes the observation data and results. Discussion is presented in Section 4, and the conclusion is presented in Section 5.

## 2. Data and Methods

The THEMIS satellites measure plasma and fields in the solar wind, near the magnetopause and in the magnetosphere. Magnetic field and plasma moments were obtained by the flux gate magnetometer, electrostatic analyzer, and solid state telescope (Angelopoulos, 2009; Auster et al., 2008; McFadden et al., 2008). The electric field was obtained by  $\mathbf{E} = -\mathbf{v} \times \mathbf{B}$ , where  $\mathbf{v}$  is the velocity moment and  $\mathbf{B}$  is the magnetic field. We have validated that the spin-plane components of  $-\mathbf{v} \times \mathbf{B}$  agree with the electric field from the EFI instrument (not shown). The time resolution is 3 s.

This study also uses the all-sky imagers (ASIs) at Inuvik (INUV), Fort Smith (FSMI), and Poker Flat (PKR) to identify dawnside discrete and diffuse aurora. ASIs are powerful tools to determine the distribution and strength of aurora and the propagation direction of aurora arcs, offering a diagnostic tool to examine particle precipitation from the magnetosphere. The time resolution is 3 s (Donovan et al., 2006; Mende et al., 2009).

The ground-based magnetometer stations at Yellow Knife (YKC) and Fort Yukon (FYKN) are located at 65.5° and 67.5° magnetic latitude, respectively, providing ground magnetic perturbations for the events. The time resolutions are 1 min for YKC and 1 s for FYKN. Other high latitude ground magnetometers are also used to get the ionospheric equivalent currents (Russell et al., 2008).

The Special Sensor Ultraviolet Spectrographic Imager (SSUSI) is a far-ultraviolet imager on board the Defense Meteorological Satellite Program (DMSP) spacecraft (Paxton et al., 2002). The DMSP satellites are Sun-synchronous, polar orbiting around the Earth, at an altitude of ~840 km. The principle component of SSUSI is a scanning imaging spectrograph (SIS) that scans the far-ultraviolet spectrum perpendicular to the spacecraft trajectory. Each scanning image is built up over 20–30 min when the satellite flies over the polar region. In this work, we use the SSUSI observation of DMSP-16 and DMSP-17 in the northern hemisphere for the first event and DMSP-18 observation in the southern hemisphere for the second event.

It is convenient to use the field-aligned coordinates (FAC) to study the propagation direction of waves. The Z component of FAC system is parallel to the local magnetic field. The Y component is the cross product of the Z component in FAC system and the radial direction, which is positive eastward. The third component, X, completes orthogonal right-handed system. The X component near the magnetic equator is close to the radial direction. The data were not averaged but linearly interpolated for the coordinate transformation.

We use the ion density to represent the plasma density in the magnetosheath, while the electron density is used in the magnetosphere. We have compared the electron density moment to the spacecraft potential density (Nishimura et al., 2013) and confirmed that the cold plasma density below the ESA energy range is negligibly small during the Pc5 activity. We obtain Pc5 signals by applying a band-pass filter between 150 and 600 s (1.67–6.67 mHz) to the measured signal. We calculate the wave frequency by using the wavelet analysis, and select the most intense frequency one as the wave frequency.

## 3. Results

### 3.1. Event 1 on 7 November 2007

Figure 1 summarizes the observations by THEMIS ASIs, THEMIS D and E in the dawnside outer magnetosphere (~6 hr MLT, Figure 1C), and YKC magnetometer for the 21 November 2007 event. The footprints of THEMIS D and E were in the FSMI field of view during the whole timespan. THEMIS A did not have plasma measurements in this event. The INUV ASI was located at ~3 hr MLT, and the FSMI ASI was located at ~6 hr MLT. Diffuse aurora was present below ~70° MLAT throughout this event (Figures 1Aa and 1Ab). Quasi-periodic brightenings of discrete arcs became visible from 13:38 UT near the poleward edge of the diffuse aurora. The arcs moved poleward repetitively with a period of ~6 min. The arc intensity did not decay monotonically but transiently increased at 13:53 UT (Figure 1Aa). The onset of the periodic auroral intensifications coincided with the onset of the Pc5 pulsations in the ground magnetometer at YKC, and the auroral intensifications had a nearly one-to-one correspondence with the Pc5 pulsations in the ground magnetic field at YKC (Figure 1Ak).

Both THEMIS D and E observed periodic oscillations (~6 min period, within the Pc5 ULF band) in the magnetic field, especially in the GSM z-component (Figure 1Ac and 1Bc). The z-component was nearly parallel to the background magnetic field, and thus the oscillations at the satellite locations were mainly compressional.  $B_x$

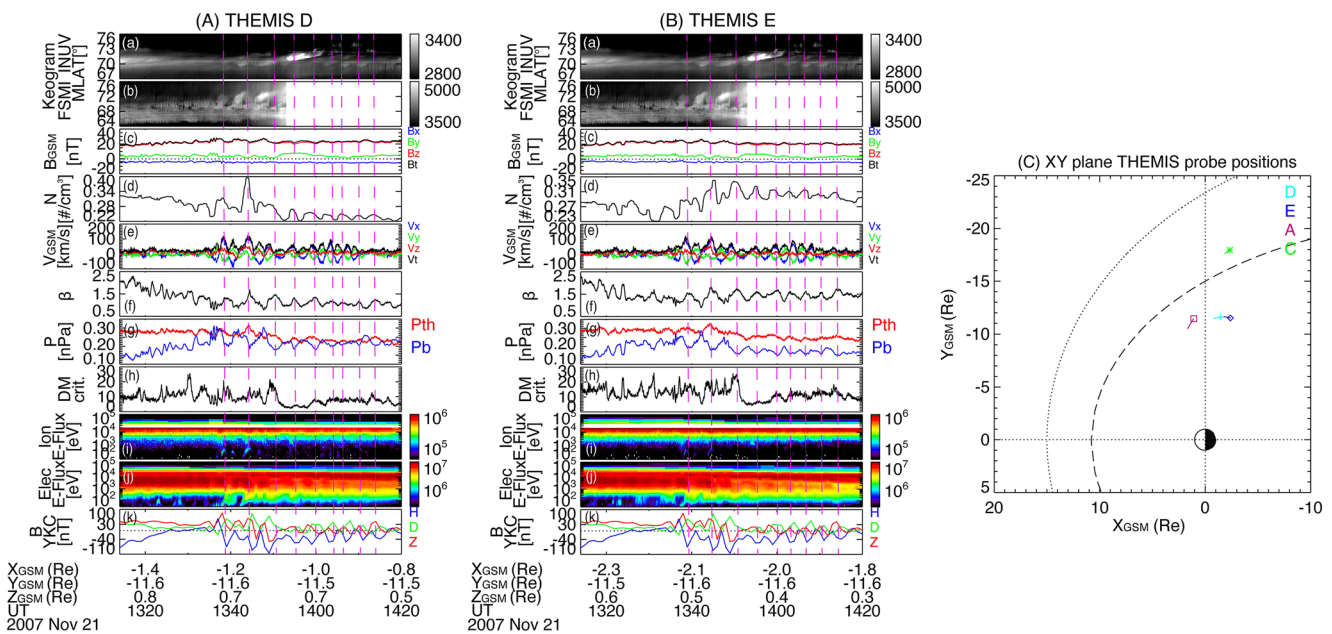


**Figure 1.** ASI keograms and magnetospheric satellite observations by (A) THEMIS D and (B) THEMIS E for the 21 November 2007 event. Panels (Aa) and (Ba) show the keogram of the INUV ASI, and panels (Ab) and (Bb) show the keogram of the FSMI ASI. Panels (Ac–Aj) show the magnetic field, plasma density smoothed over one-minute, flow velocity, beta, thermal and magnetic pressures, drift mirror instability parameter, and electron and ion energy fluxes at THEMIS-D. Panels (Bc)–(Bi) are in the same format except for THEMIS-E. Panels (Ak) and (Bk) are the ground magnetic field at YKC. Panel (C) shows the orbits of THEMIS satellites in the GSM X-Y plane between 13:14 and 14:20 UT.

and  $B_y$  were much smaller than  $B_z$ .  $\beta$  ( $P_i/P_b$ , Figures 1Af and 1Bf) was above  $\sim 1$ , and the drift mirror instability parameter ( $\beta_\perp(P_\perp/P_\parallel - 1)$ , Figures 1Ah and 1Bh) (Nykyri et al., 2021) was much larger than 1, indicating that the satellites were in the central plasma sheet and the drift mirror mode waves were unstable. THEMIS D had slightly smaller  $\beta$  ( $\sim 1.2$  after 13:38 UT) compared with THEMIS E ( $\sim 1.5$  after 13:38 UT), suggesting that THEMIS E was slightly closer to the neutral sheet than THEMIS D. The vertical lines mark individual peaks of  $\beta$  oscillations after 13:38 UT. The oscillations in the thermal pressure and magnetic pressure were in anti-phase (Figures 1Ag and 1Bg), and thus the oscillations were not the fast-mode waves but possibly the slow or drift mirror mode waves. The individual peaks in the  $\beta$  oscillations overall corresponded with the dips of the auroral intensity oscillations, as well as the dips of the  $H$ -component of the magnetic field at YKC. The plasma velocity also showed clear Pc5 oscillations (Figures 1Ae and 1Be), and  $V_x$  had a phase lag from  $B_z$ . The phase relation is investigated more in detail later in this section. The energy flux (Figures 1Ai and 1Aj) includes both SST and ESA observations. The plasma density oscillations reflected modulations of electrons and ions with several hundreds of eV, but they were not in-phase with  $P_i$ , suggesting that the low-energy plasma did not largely contribute to the thermal pressure but perhaps represented other plasma sources. The high energy plasma sheet ions and electrons ( $\geq 1$  keV) corresponded well with  $P_i$ , and they were the major contributor to the thermal pressure.

To further investigate the Pc5 wave properties at THEMIS D as a representative satellite in the dawnside magnetosphere, we show the Pc5-filtered total magnetic field, Pc5-filtered thermal pressure, and the phase difference between the magnetic field and thermal pressure in Figure 2A. The total magnetic field spectrum showed a peak frequency at 2.8 mHz and had signals confined below 6 mHz after 13:30 UT. The thermal pressure, on the other hand, was mainly enhanced at 13:30–14:05 UT with a peak frequency at 3.1 mHz. The Pc5 waves were enhanced within the Pc5 frequency range (1.67–6.67 mHz) and thus it is appropriate to use the Pc5 band-pass filter to extract the Pc5 wave signal. The thermal pressure and the total magnetic field showed a good anti-correlation ( $\sim -180^\circ$  phase lag, Figure 2Ae) during the largest Pc5 magnetic field amplitude ( $\sim 13:40$ – $13:50$  UT). The anti-phase relation again indicates that the Pc5 waves at the satellite locations were not in the fast-mode but the slow or drift mirror mode. After 14:00 UT, the phase lag became between  $-180^\circ$  and  $-90^\circ$ . Similar properties were seen at THEMIS E but are not shown here.

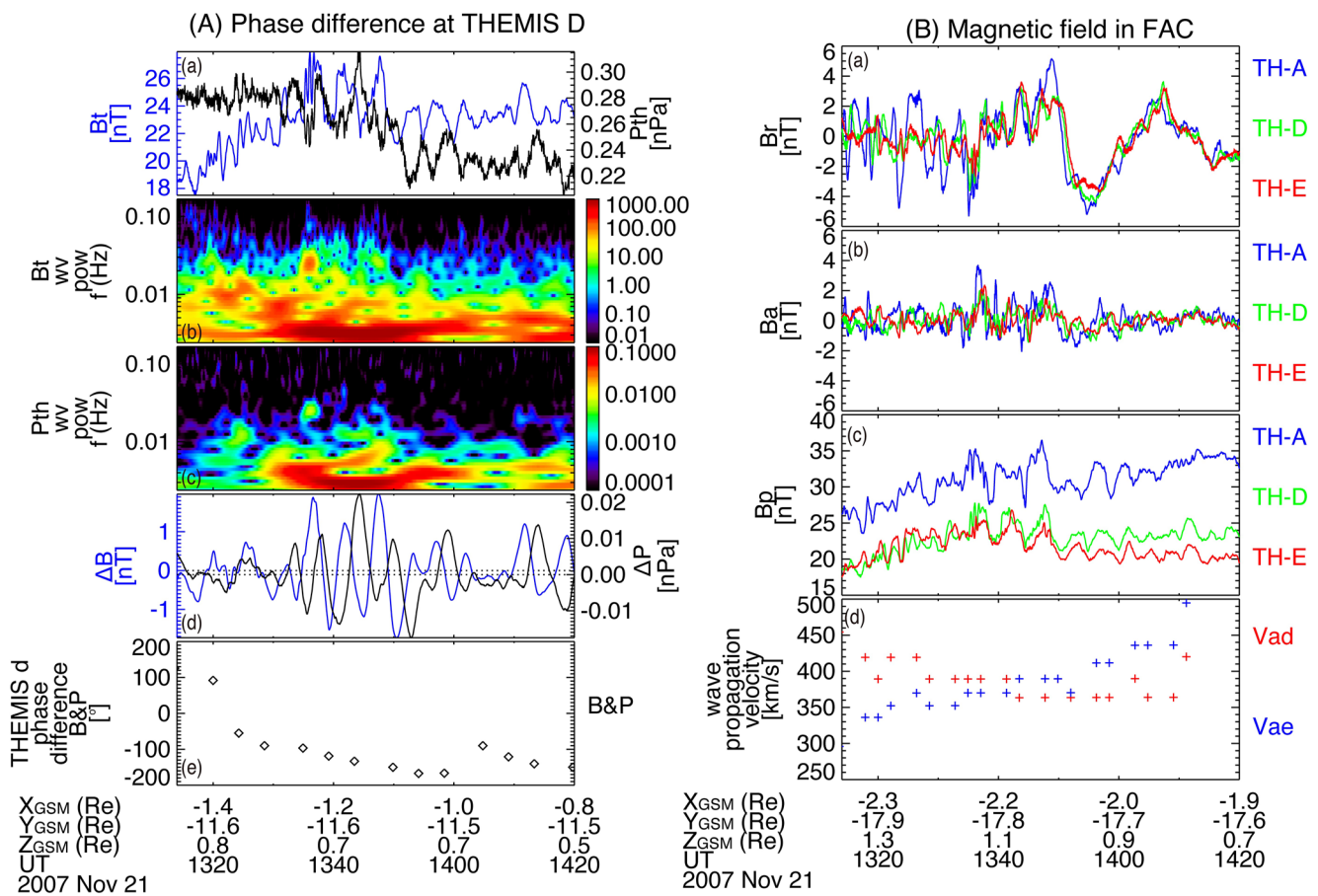


**Figure 2.** Panel (Aa) shows the total magnetic field and thermal pressure. (Ab) and (Ac) show their frequency spectra. Panel (Ad) shows the Pc5 filtered total magnetic field and thermal pressure and panel (Ae) shows their phase difference. Panels (Ba–Bc) show the magnetic field components in the FAC coordinate system for THEMIS A, D, and E. Panel (Bd) shows the propagation velocities from THEMIS A to E and from THEMIS A to D in red and blue crosses, respectively.

As shown in Figure 1C, THEMIS A, D, and E were nearly aligned with the GSM  $x$ -axis. From the magnetic field data at the three satellites, we calculated the wave propagation velocity along the satellites (Figure 2Bd). The magnetic field data at three satellites in the FAC system are shown in Figures 2Ba–2Bc. The signals were dominated by the parallel component and the radial magnetic field also showed considerable Pc5 oscillations. The time lags of the signal between two satellites are calculated by finding the maximum correlation coefficient of the parallel magnetic field component in the Pc5 frequency range. The calculation window is 50 min to include several wave periods, and the time step is 3 min. The calculated time lag has a coefficient of  $\sim 0.7$ , which is larger than other local maximums by 0.3. On average, the magnetic field at THEMIS A was ahead of D by 42 s, and ahead of E by 58 s. The parallel component of the magnetic field suggests that the calculated time delays are reasonable. The satellite separations were 16,506 (THEMIS A-D) and 22,436 (THEMIS A-E) km, and thus the calculated propagation velocity was  $\sim 400$  km/s tailward (from THEMIS A through D to E). Because THEMIS A was located close to the nominal dawnside magnetopause (Figure 1C), this propagation direction indicates that the waves originated in the dawnside magnetopause and propagated anti-sunward. This propagation direction is consistent with the Poynting flux analysis (Figure 3d), and thus it is reasonable to estimate the velocity from current satellite orientation. This propagation speed was much less than the local Alfvén speed ( $\sim 850$  km/s) and fast-mode speed ( $\sim 1,200$  km/s), but faster than the plasma flow speed ( $\sim 100$  km/s, Figure 1Ae). Thus the waves were not primarily in the fast-mode, Alfvén waves or by local convection. Because 400 km/s is larger than the typical drift mirror mode wave velocity ( $< 100$  km/s) (I. J. Rae et al., 2007; Walker et al., 1982), the wave propagation is governed by another wave mode. This issue is discussed later in this section.

To discuss the phase relation between the electric and magnetic fields and Poynting flux, we show in Figure 3 the electric and magnetic fields in the Pc5 frequency range in the FAC system, the phase difference for their

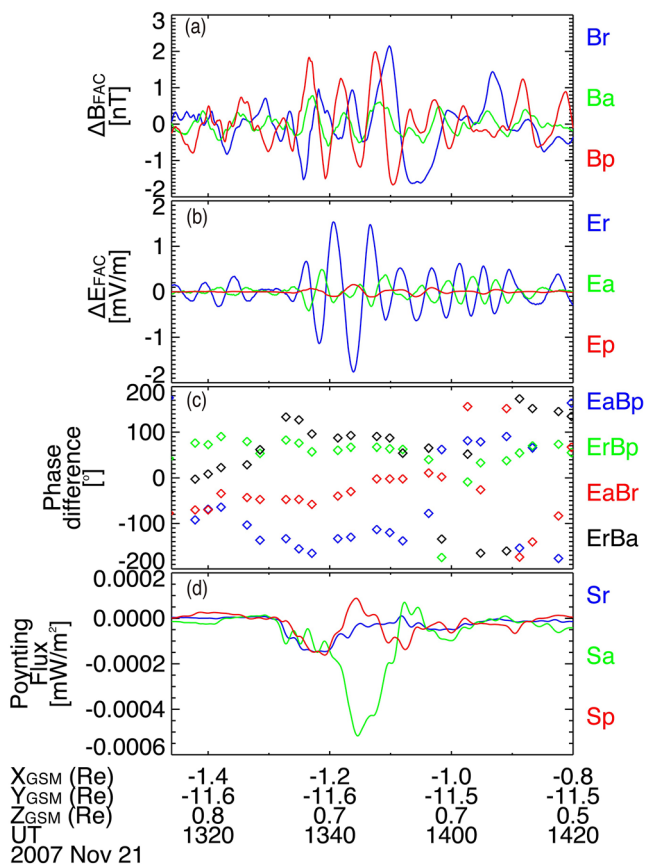


**Figure 3.** Pc5-filtered (a) magnetic and (b) electric field data in the FAC coordinate system, (c) phase difference of the major components of the magnetic and electric field, and (d) the Pc5-filtered Poynting flux at THEMIS D.

major components, and the Pc5-filtered Poynting flux. The electric field was obtained from the plasma flow moment as  $\mathbf{E} = -\mathbf{v} \times \mathbf{B}$ . At THEMIS D, the Poynting flux was almost zero before 13:31 UT due to the small electric and magnetic fields. After that, the parallel magnetic field ( $B_p$ ) and radial electric field ( $E_r$ ) became the dominant components. Considerable magnitudes of the radial magnetic field ( $B_r$ ) and azimuthal electric field ( $E_a$ ) were also present. The phase difference between  $E_r$  and  $B_p$  was less than 90°, leading to a substantial azimuthal Poynting flux ( $S_a$ ). The phase difference between  $E_r$  and azimuthal magnetic field ( $B_a$ ) was around 90° and the phase difference between  $E_a$  and  $B_r$  was variable and mostly between -90° and 0°. Those two components gave the parallel Poynting flux ( $S_p$ ) oscillating around zero. The oscillations of  $S_p$  (~3 mHz) indicate that part of the energy was converted to Alfvén waves and bounced back and forth between the two hemispheres as standing waves.  $E_a$  and  $B_p$  were out-of phase (between -180° and -90°) during 13:31–13:51 UT. The Poynting flux perpendicular to the magnetic field was westward and inward at 13:31–13:41 UT, and then became mostly westward after 13:41 UT. This Poynting flux direction is consistent with the wave propagation direction estimated by the timing analysis and indicates that the electromagnetic energy flowed from the dawnside magnetopause toward the nightside magnetosphere.

To investigate behavior of the dawnside magnetopause for this event, we present the observations by THEMIS C in Figure 4A. THEMIS C was mainly in the magnetosheath until 13:51 UT and then mainly in the magnetosphere. However, THEMIS C encountered magnetopause crossings. The vertical lines mark magnetopause crossings based on abrupt changes in the ion and electron energies and magnetic field. The regions with tailward  $V_x$  (up to 400 km/s), larger density, larger dynamic pressure in the regions of cooler ions and electrons indicate that those regions are the magnetosheath. The regions with slower  $V_x$ , lower density in hotter ions and electrons correspond to the magnetosphere. The period of the oscillations after 13:51 UT was about 6 min. This period is consistent with the ULF pulsations that were seen in aurora (Figures 4Aa and 4Ab) and ground magnetometer data (Figure 4Aj). Given the spacecraft orbital velocity was much slower than the flow velocity, the observed oscillations were most probably caused by magnetopause surface waves (Kavosi & Raeder, 2015).

The large propagation velocity (~400 km/s) in the magnetosphere could be explained by the magnetopause surface wave propagation. Based on the wave period (~352 s), a quarter of the wavelength at THEMIS D was 35,200 km (~5.5  $R_e$ ), which was comparable to the distance from THEMIS D to the magnetopause (~5  $R_e$ , Figure 1C). Thus, with large wave amplitude, the magnetopause surface waves were capable of modulating the plasma at THEMIS satellites in the magnetosphere, making them satisfy the drift mirror instability threshold and generate waves (Nowada et al., 2009; I. Rae et al., 2007; Walker et al., 1982). The magnetosheath flow speed (~400 km/s) was comparable to the anti-sunward velocity in the magnetosphere (~400 km/s). Thus, the wave speed in the magnetosphere was not the actual propagation velocity of drift mirror waves but could be related to the anti-sunward motion of the magnetopause surface waves at the magnetosheath flow speed. The simultaneous observations at the magnetopause, magnetosphere and ionosphere provide evidence that the dawnside magnetopause oscillations were the source of the ULF pulsations of this event, and the signal was converted to the Alfvén waves traveling to the ionosphere and drift mirror or slow mode waves propagating into the dawnside magnetosphere (Chaston et al., 2005; Chen & Hasegawa, 1974; Fujita et al., 1996).

Figure S1 in Supporting Information S1 shows the THEMIS C observation from 13:55 to 14:20 UT. The “more magnetosheath region” is marked in red and “more magnetospheric region” is marked in blue at the top of the figure. The higher density and lower temperature are in the magnetosheath side, and vice versa. The total pressure ( $P_i + P_{ele} + P_B$ , where  $P_{ele}$  is the electron pressure) variations in Figure 4Ag and Figure S1g in Supporting Information S1 reach local maxima around the boundaries between magnetosphere and magnetosheath. This is

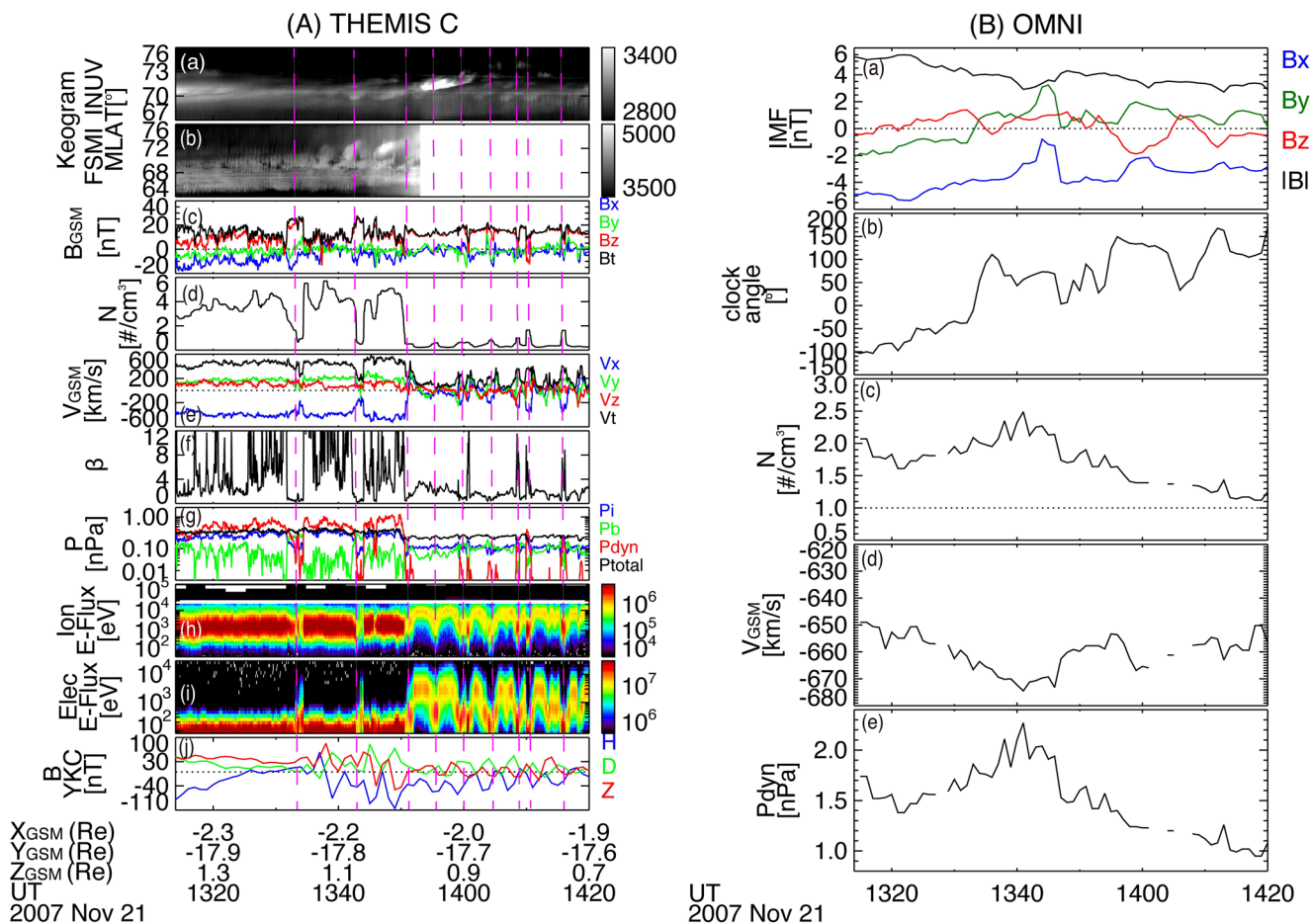


**Figure 4.** THEMIS C observations in the same format as Figure 1, except for an addition of the dynamic pressure and total pressure in panel (Ag). The vertical lines mark the magnetopause crossings. Panels (Ba–Be) show the IMF, IMF clock angle, solar wind density,  $x$ -component of the solar wind velocity in GSM, and dynamic pressure from the OMNI data.

expected for surface waves generated by KH instability because the centrifugal force is balanced by the pressure force at the quasi-stationary state (Hwang et al., 2011). The oscillations of tailward plasma flow ( $V_x$ ) with slower velocity were probably because of the vortical motion of a mixture of magnetosheath and magnetosphere plasma, which is another key feature of the surface waves (M. O. Archer et al., 2022). Thus we infer that the generation mechanism for the waves in the magnetosphere was the magnetopause surface waves.

The solar wind condition from OMNI data are shown in Figure 4B. The IMF was dominated by the negative  $B_x$  component. The IMF  $B_z$  fluctuated near zero and the IMF  $B_y$  turned from negative to positive at 13:33 UT. Corresponding to this  $B_y$  turning, the clock angle turned from  $\sim 90^\circ$  to  $\sim 90^\circ$  at 13:33 UT. Because of the changes in the plasma density, the dynamic pressure showed a longer oscillation with a period of 8 min. Thus, the dynamic pressure pulses might contribute to some of the wave intensification, but they were unlikely to be the dominant driver of the long-lasting Pc5 waves since these waves are not immediately following the dynamic pressure variations. The  $\sim 90^\circ$  clock angle is a favorable condition for KH instability (Kavosi & Raeder, 2015). We suggest that the IMF  $B_y$  turning provided a seed fluctuation for the KH instability at the dawnside magnetopause and may be related to the dawn-dusk asymmetry that is discussed in Figure 5. KH instability further generated the surface waves propagating anti-sunward along the magnetopause. The simulation by Tang et al. (2013) showed that KH instability can be excited at the flanks during a radial IMF, and the observations by Shi et al. (2018) also suggested KH instability occurs in  $B_x$ -dominant IMF.

As mentioned above, Pc5 waves can have a dawn-dusk asymmetry (Baker et al., 2003; I. Rae et al., 2005; Vennerstrøm, 1999; Zhao et al., 2020). Figure S3 in Supporting Information S1 shows the high-pass filtered

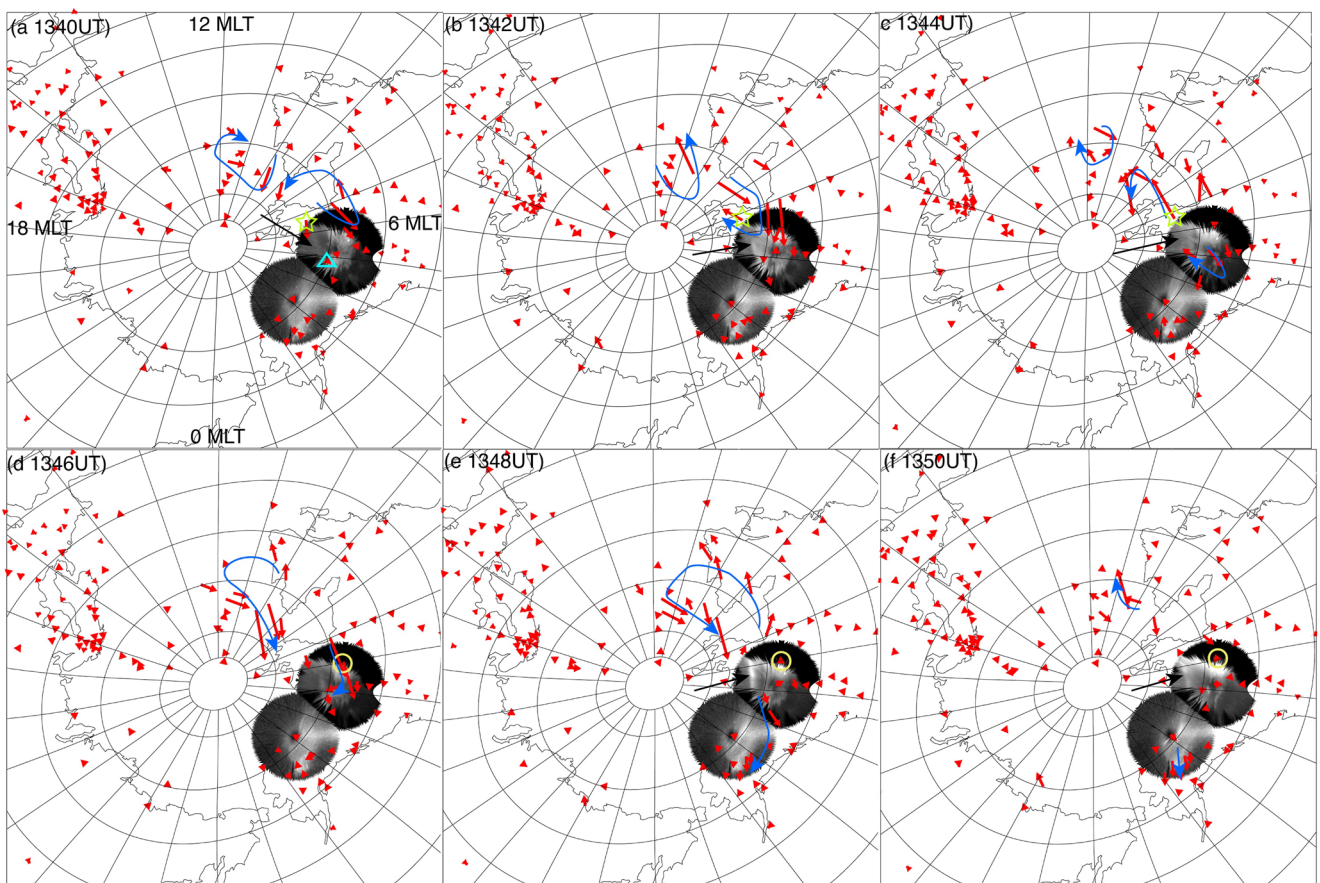


**Figure 5.** Selected snapshots of equivalent ionospheric current vectors from ground magnetometers overlaid onto the ASI data of FSMI and INUV for the 21 November 2007 event. The red arrows show the direction and magnitude of equivalent currents. The blue arrows schematically indicate the current vortices. The yellow pentangles and circles mark the BLC and the RAL station, respectively. The light blue triangle marks the YKC station in the first panel. The magnetic local times are indicated in the first panel.

(<600s) magnetometer data at 6 selected stations (YKC, GIM, T29, IVA, AMD, and NOK). The stations are located between 65 and 70 MLAT and their approximate MLTs at the 13:00 UT are noted in each panel. This figure clearly shows the dawnside Pc5 waves were much stronger than the duskside Pc5 waves. We also use the ionospheric equivalent currents and the auroral imaging to study the global distribution of Pc5 waves. Figure 5 shows six snapshots of ASIs at INUV and FSMI and equivalent current vectors in the northern hemisphere, taken every 2 min from 13:40 to 13:50 UT. The ground magnetometer data with 1 min resolution from SuperMAG were detrended over 10 min. The red vectors indicate the strength and direction of equivalent currents by rotating horizontal magnetic field perturbations by 90° clockwise and their initial points are located at ground magnetometer stations. Figure S2 in Supporting Information S1 shows the open-closed boundary (OCB) (green line) from the Tsyganenko model. The THEMIS A, D, and E footprints are located by magenta, cyan, and blue squares. The footprints of satellites and the center of current vortices were all equatorward than the OCB. This time span includes the three brightenings of the Pc5 auroral arcs (13:40, 13:42–13:44, and 13:48–13:50 UT) as highlighted by the black arrows, which were brighter at dawn (FSMI ASI) than pre-dawn (INUVT ASI). The first arc was very faint but with large equivalent currents in the morning sector. The second arc was visible between 13:42 and 13:44 UT with higher intensity and the brightest arc occurred at 13:48 UT. All the three arcs showed evident propagation. For example, the arc was located at 72°–73° MLAT at 13:48 UT and then at 74°–75° MLAT with fading brightness, showing a poleward motion. Throughout the event, the currents were mainly enhanced between the pre-dawn (Alaska) and noon (Greenland) sectors and were largest at pre-noon. The currents on the dawnside were much larger than the duskside and mostly perturbed between 65° and 75° MLAT. The dawn-dusk asymmetry of the current distribution is strikingly different from the Pc5 wave events studied by Motoba et al. (2003) and Shi et al. (2020), where Pc5 waves in their events had substantial amplitudes on the duskside. This dawn-dusk

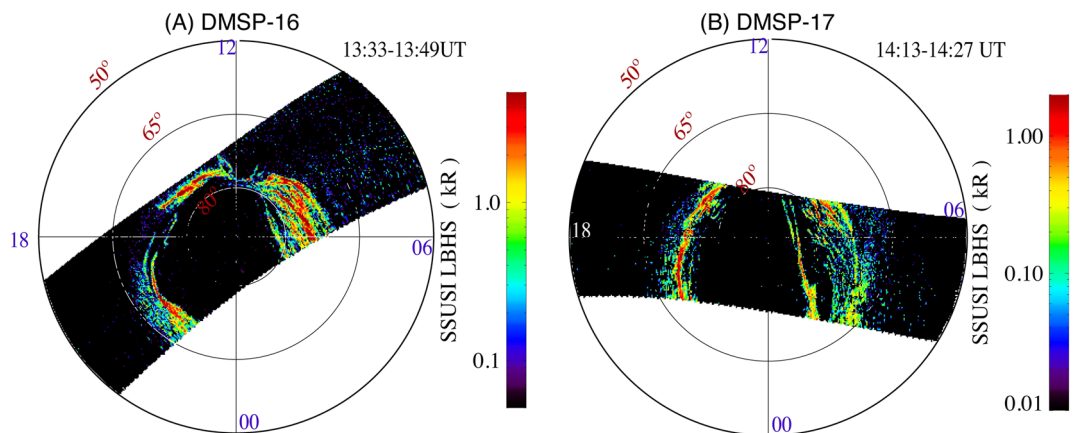


**Figure 6.** The SSUSI observations for the northern hemisphere during (A) 13:33–13:49 UT (DMSP-16) and (B) 14:13–14:27 UT (DMSP-17). The color indicates the auroral intensity.

asymmetry is also consistent with the previous study which demonstrated stronger dawnside Pc5 wave activity (Gillies et al., 2018; I. Rae et al., 2005). The currents in the predawn sector were weak in Figures 5a and 5b and then increased in Figures 5c, 5e, and 5f. This current enhancement at predawn was associated with the discrete auroral pulsations at INUV.

During the whole process, the currents poleward of the discrete arcs rotated clockwise, while the currents equatorward of the arcs rotated counterclockwise. For example, the current at Baker Lake (BLC, marked as a yellow pentangle) was directed westward at 13:40 UT, poleward at 13:42 UT, and eastward at 13:44 UT, forming a clockwise rotation. The current direction at Rabbit Lake (RAL, marked as a yellow circle) was westward at 13:46 UT, sunward at 13:48 UT, and eastward at 13:50 UT, forming a counterclockwise rotation. This current polarization reversal is consistent with the phase reversal below and above FLR latitude (Chen & Hasegawa, 1974; Southwood, 1974).

The polarization pattern is related to the distribution of equivalent currents. As highlighted by the blue arrows, the equivalent currents had multiple vortices on the dawnside. At 13:40 UT, a counterclockwise current vortex emerged in the morning sector with its center around  $74^{\circ}$  MLAT, while a clockwise vortex appeared at prenoon. Two minutes later, these two vortices had reversed polarities. At 13:44 UT, the polarities reversed again, and another clockwise vortex appeared at predawn. At 13:46 UT, when there was no visible auroral arc, the currents in the morning sector formed a large counterclockwise vortex, and the predawn currents became weaker and almost linearly polarized. Associated with the brightest arc, the currents in the morning sector had a large counterclockwise vortex centered around  $76^{\circ}$  MLAT at 13:48 UT, while the currents in the predawn sector showed a partial clockwise vortex. At 13:50 UT, the currents became much smaller with almost linear polarization in the predawn sector and at prenoon. The multiple vortices pattern of the equivalent currents on the dawnside is quite different from the Pc5 wave events studied by Motoba et al. (2007), whose current cells appeared on both dawn and dusk sides. The vortices on the dawnside indicate that the dawnside currents in Pc5 range are closed on the dawnside rather than through the duskside.

Since the THEMIS ASIs only provided auroral observations on the dawnside, we show the Special Sensor Ultraviolet Spectrographic Imager (SSUSI) data of DMSP 16 and 17 in Figure 6 to examine whether aurora also had the dawn-dusk asymmetry. DMSP-16 and 17 crossed the auroral oval in the northern hemisphere in the beginning and ending part of the Pc5 pulsations, respectively. At both time intervals, it is evident that the dawn-dusk auroral activity was highly asymmetric. In the morning sector, the aurora activity was much stronger and had multiple arcs with a roughly azimuthal orientation. The arc orientation is consistent with the ASI observations. Since the ASIs only detected an arc at a time, the presence of the multiple arcs in the SSUSI data is because SSUSI scanned the quasi-periodic occurrence of the poleward-moving arcs on the moving platform. The duskside auroral oval was thinner and had only one or two major arcs at each local time. The fewer arcs on the duskside indicate that the Pc5 wave activity on the duskside was much weaker.

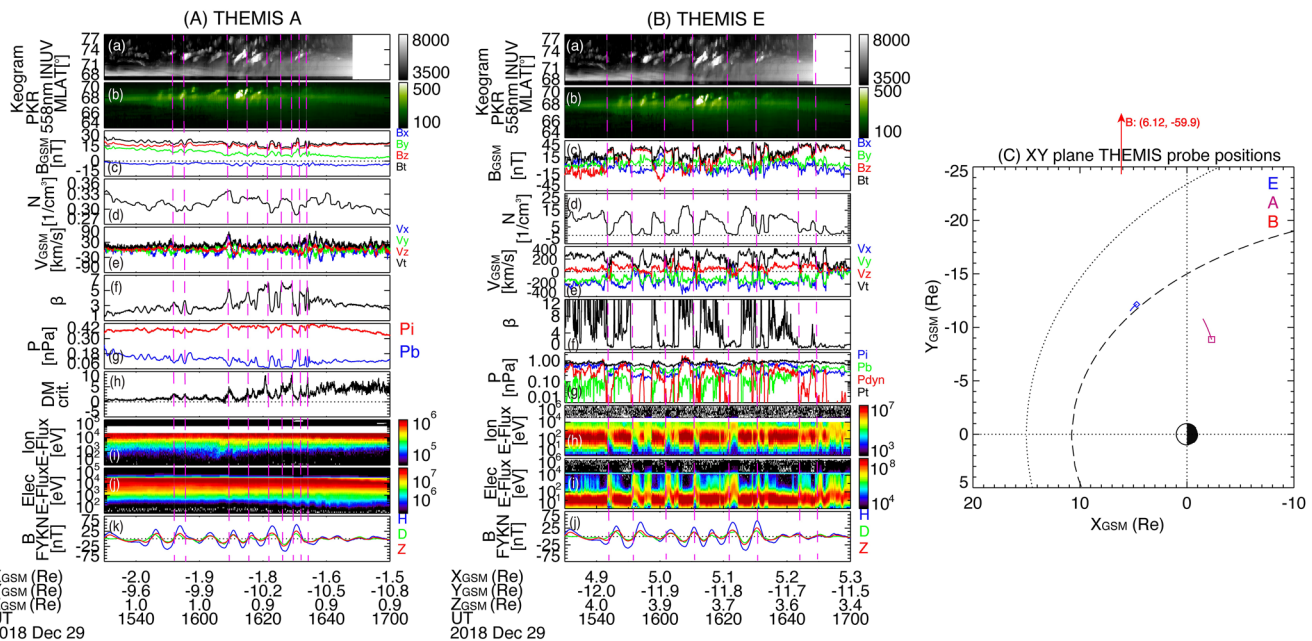


**Figure 7.** ASI keograms and magnetosospheric satellite observations by (A) THEMIS A and (B) THEMIS E for the 29 December 2018 event. Panels (Aa and Ba) show the keogram of the INUV ASI, and panels (Ab and Bb) show the keogram at 558 nm of the PKR ASI. Panels (Ac–Aj) show the magnetic field, plasma density smoothed over 1 min, flow velocity,  $\beta$ , ion, magnetic, dynamic pressures, drift mirror instability parameter, and ion and electron energy spectrum at THEMIS-A. Panels (Bc–Bi) are in the same format of Figure 4a for THEMIS-E. Panels (Ak and Bj) are the ground magnetic field at FYKN in the  $P_c 5$  frequency range. The vertical lines mark the major peaks of  $\beta$  at THEMIS A and magnetopause crossings for THEMIS E. Panel (C) shows the THEMIS satellite orbits. THEMIS A, E, and B were in the magnetosphere, magnetosheath, and solar wind, respectively.

### 3.2. Event 2 on 29 December 2018

To examine whether the findings in the first event are coincidental or can also be seen in another event, we investigated  $P_c 5$  waves that occurred on 29 December 2018. Figure 7 presents the data from THEMIS A and E, ASI data at INUV and PKR, and ground magnetometer data at FYKN, as well as the satellite locations of this event. According to the keograms, diffuse aurora was observed below  $68.5^\circ$  MLAT throughout the event, and discrete auroral arcs propagated poleward quasi-periodically during 15:50–16:40 UT.

THEMIS A was located in the dawnside outer magnetosphere. Figure 7A shows that the  $P_c 5$  oscillations (about 7 min) are visible in  $B_z$ , plasma density,  $\beta$ , magnetic pressure, high energy portion of the energy spectrograms and the ground magnetic field. The vertical lines mark the major peaks of  $\beta$  oscillations, and they generally corresponded well with the dips of the auroral arc intensity oscillations and had a nearly  $90^\circ$  phase shift from the ground magnetic field. The density and the high energy ions both had an anti-phase relation with  $\beta$ , indicating that the energetic particles represented the thermal pressure.  $B_z$  and the plasma pressure were anti-phase with  $\beta$ .  $\beta$  had a large value ( $\sim 3$ ) when observing intense discrete arcs in keogram, and the drift mirror instability parameter was much larger than 1 after 15:50 UT (Nykyri et al., 2021). Similar to the previous event, the high  $\beta$  value, high drift mirror instability parameter and anti-correlation between the thermal and magnetic pressures suggest slow or drift mirror mode waves. The flow velocity showed oscillations at a higher frequency perhaps because of the second harmonic waves (Liu et al., 2009).

THEMIS E was located near the model magnetopause (Figure 7C). The vertical lines in Figure 7B mark magnetopause crossings based on the jumps in  $B_z$ , plasma density and ion and electron energy. The magnetosheath can be identified as tailward  $V_x$  (200–400 km/s), large density ( $\sim 10 \text{ cm}^{-3}$ ), large dynamic pressure, and cooler ions and electrons. Positive  $B_z$  with low density and slow  $V_x$  in hotter ions and electrons correspond to the magnetosphere. Unlike the first event, THEMIS E stayed close to the magnetopause and fully crossed the magnetopause multiple times. The dawnside magnetopause oscillations in the  $P_c 5$  range again suggest that the dawnside magnetopause surface waves were the driver of the  $P_c 5$  pulsations for this event. Similar to the first event, the total pressure around the boundaries was at the local extreme value, indicating the event was related to KH instability in the magnetosheath.

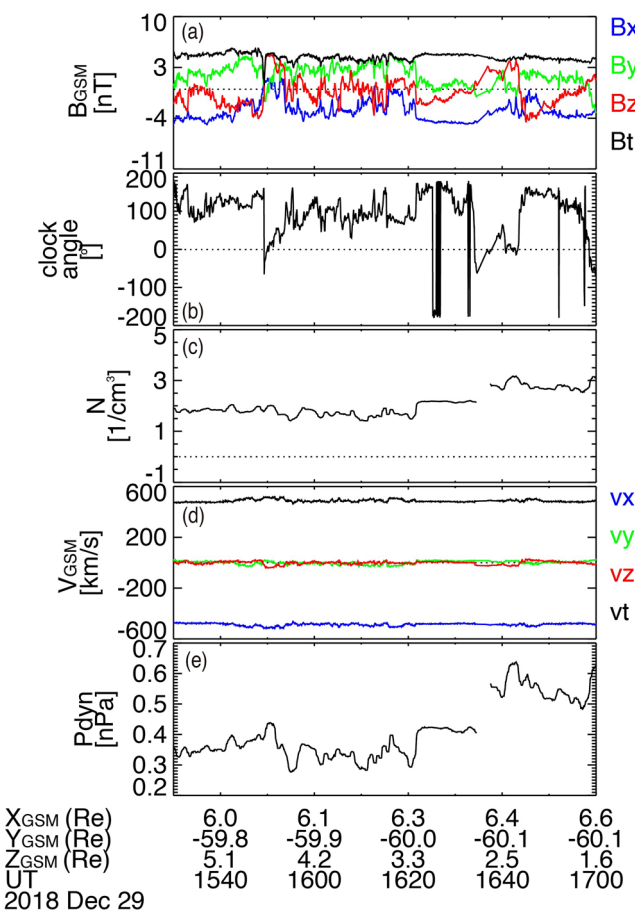


**Figure 8.** Panels (a–e) show the IMF, clock angle, plasma density, flow velocity and dynamic pressure at THEMIS B in the solar wind.

16:13 UT showed a poleward and westward propagation. The arcs during 16:15–16:19 UT showed a similar propagation with a less obvious westward motion. The westward arc motion may be related to the westward Poynting flux in the magnetosphere.

The equivalent currents were much smaller on the dusk side than the dawnside throughout the event. At 16:09 UT, the currents had a clockwise polarization in the morning and predawn sectors, while a smaller counterclockwise vortex emerged in the postdawn sector. At 16:11 UT, the currents had a counterclockwise sense vortex in the morning sector and an eastward polarization in the predawn sector at high latitude (above 70° MLAT). At 16:13 UT, the currents formed a large counterclockwise vortex in the morning sector and a clockwise one in the predawn sector. The currents at 16:15 UT had two comparable vortices with opposite polarization sense in the morning sector and the predawn currents became much weaker. At 16:17 UT, the currents had partial of clockwise, counterclockwise, and clockwise polarization in the morning, postdawn, and predawn sector, respectively. At 16:19 UT, the currents formed a counterclockwise vortex in the morning sector and clockwise vortex with a larger current magnitude in the predawn sector. The occurrence of multiple current vortices is consistent with the previous event. Thus this Pc5 wave event can also be characterized by the alternating polarities of the currents on the dawnside. The Pc5 currents were mainly located between 67° and 78° MLAT, which corresponded to the discrete arcs. The arcs likely highlighted the upward FACs of the Pc5 current system.

The SSUSI observations are shown in Figure 10g. Similar to the Pc5 equivalent currents, the auroral activity was also highly asymmetric. The auroral oval in the dawn sector was wider and had multiple arcs with approximately east-west orientation (tilted poleward toward noon), while the auroral oval on the duskside was thinner and only had one or two major arcs. The dawnside arc location and orientation were consistent with the ASIs data, and

THEMIS B was immersed in solar wind (Figure 7C) and provided the condition of the solar wind for this event. Figure 8 shows the IMF, the clock angle, plasma density, flow velocity and dynamic pressure at THEMIS B. The dynamic pressure had oscillations before 16:25 UT, and thus it is possible that dynamic pressure oscillations contributed to this Pc5 wave event partly. The IMF was dominated by the negative  $B_x$  and positive  $B_y$  components, with nearly zero  $B_z$  on average. The clock angle stayed around 100° except for brief excursions. Although the IMF was not strongly northward in this event, the large IMF  $B_y$  orientation is also favorable for KH instability growth in the magnetosheath (Kavosi & Raeder, 2015), and may have contributed to its dawnside occurrence.

Owing to the limited availability of satellite data in the magnetosphere, the wave propagation velocity could not be calculated for this event. To infer wave properties, we investigated the phase relation between the Pc5-filtered magnetic and electric fields and the Poynting flux at THEMIS A as shown in Figure 9. During the event at 15:50–16:25 UT, the parallel magnetic field ( $B_p$ ) and radial electric field ( $E_r$ ) were dominant but with considerable radial magnetic field ( $B_r$ ) and azimuthal electric field ( $E_a$ ) components. The average phase difference between  $E_r$  and  $B_p$  was about 30°, and the compressional signal dominantly propagated westward, as can be seen as the negative azimuthal Poynting flux ( $S_a$ ). The phase difference between  $E_a$  and  $B_p$  was overall larger than  $\pm 90^\circ$ , giving a radially inward Poynting flux. Considering that THEMIS A was located in the dawnside outer magnetosphere, the electromagnetic energy flow was again from the dawnside magnetopause to the nightside magnetosphere. The phase differences for  $E_r B_a$  and  $E_a B_r$  were near  $\pm 90^\circ$ , and the parallel Poynting flux oscillated around zero, suggesting that THEMIS A measured standing Alfvén waves near the field-line resonances (FLRs) of the Pc5 pulsations with a frequency at 3 mHz.

The spatial distribution of the Pc5 activity during 16:09–16:19 UT on 29 December 2018 was also studied with six snapshots of Pc5-filtered equivalent current vectors in the northern hemisphere as well as the ASIs at FYKN and PKR every 2 min in Figures 10a–10f. The brightest arcs from 16:11 to

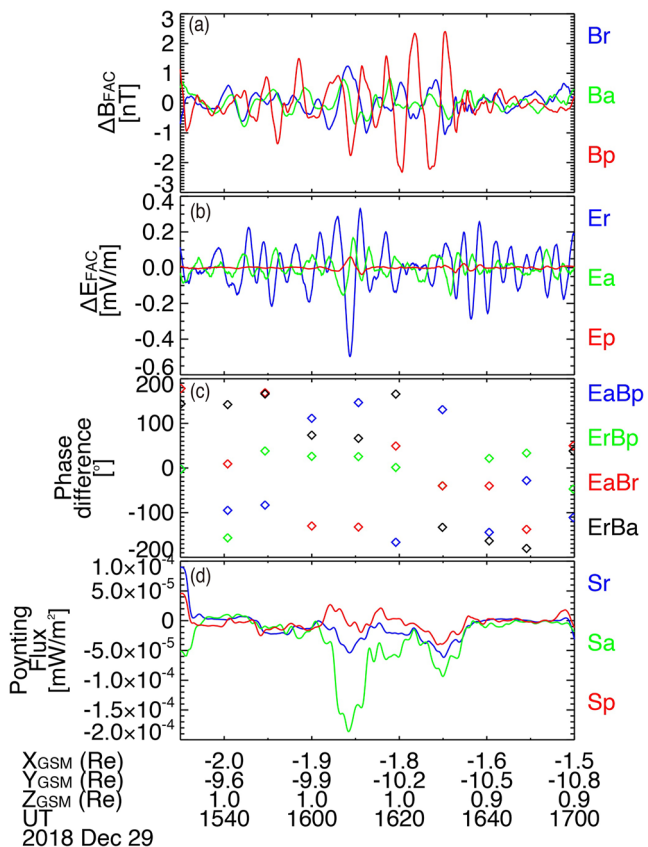


**Figure 9.** Same as Figure 3 but for THEMIS A for the 29 December 2018 event.

the presence of the multiple arcs in the SSUSI data likely corresponded to quasi-periodic occurrence of the poleward-moving arcs.

#### 4. Discussion

Past studies showed that ionospheric equivalent currents during Pc5 wave events form a twin-vortex pattern that is approximately symmetric with respect to the noon-midnight meridian and is modulated at the Pc5 frequency (Motoba et al., 2003, 2007; Wang et al., 2020). However, the equivalent currents in our study (Figures 5 and 10) were localized on the dawnside with multiple vortices of alternating polarities. This dawn-dusk asymmetry can be interpreted in terms of the dawn-dusk asymmetry of KH instability at the magnetopause. Takahashi, Hartinger, et al. (2015) concluded that the Pc5 dawn-dusk asymmetry at high latitude is a consequence of the asymmetry of the Pc5 occurring in the magnetosphere, which can be related to dawnside KH instability along the magnetopause (Shi et al., 2020). KH instability is suggested to be stabilized in the quasi-perpendicular shock region because the tangential component of magnetic field in the magnetosheath is enhanced (Nykyri, 2013). Considering that the IMF orientation in the two events was  $(-B_x, +B_y)$ , the duskside magnetopause was expected to be stable for KH instability. The dawnside magnetosheath had a more favorable condition for KH instability growth under large IMF  $B_y$  (Kavosi & Raeder, 2015), and generated magnetopause surface waves, which propagated toward nightside magnetosphere and converted to the slow or drift mirror mode waves in the dawnside outer magnetosphere. The dawn-dusk asymmetry of ionospheric equivalent currents has been rarely reported, and we suggest that the multiple current vortices and auroral arcs are the ionospheric signatures of ULF waves, which is probably related to KH instability at the magnetopause.

Anti-phase variations between the thermal pressure and the magnetic pressure are one of the key features of drift mirror mode waves in the homogeneous plasma, while in the inhomogeneous plasma, some other modes can

potentially show such property. Chen and Hasegawa (1991) and Chan et al. (1994) showed that Alfvén-ballooning modes, coupling of shear Alfvén and slow mode waves, could have an anti-phase relation, similar  $\beta$ , pressure anisotropy, and the standing signal could show such anti-phase relation with a standing Alfvén mode wave in the condition of relatively low-beta value and/or mild anisotropy. However, the vital parameter instability parameter  $\tau = 1 + \beta_{\perp} \left( 1 - \frac{\beta_{\perp}}{\beta_{\parallel}} \right)$  (Cheng & Qian, 1994) is not satisfied for the Alfvén-ballooning mode waves (the ballooning-mirror mode is possible). Moreover, our propagation velocity analysis showed that the wave propagation speed ( $\sim 400$  km/s) is much less than the fast-mode speed ( $\sim 1,200$  km/s). Thus it is unlikely that fast-mode waves in plasma inhomogeneity are the cause of the anti-phase relation. Fast waveguide mode waves when the magnetopause driver is turned on can radially propagate and have an antisunward velocity of 400 km/s (Elsden & Wright, 2015; Samson et al., 1992). Thus, waveguide mode waves coupled to FLR with a driver of magnetopause disturbance can explain the observed Poynting flux and calculated velocity. However, the antiphase between  $P_{th}$  and  $P_B$  and the drift mirror criteria make the slow or drift mirror mode waves more likely in the magnetosphere.

The equivalent currents poleward and equatorward of the discrete arcs had opposite polarities. This polarization reversal is consistent with the FLR theory. With maximum wave amplitude at the resonance location, stations poleward and equatorward of the resonance locations show opposite polarities (Chen & Hasegawa, 1974; Southwood, 1974). The local FLRs frequency is  $\sim 3$  mHz for both events, similar with the previous research in the morning section (Chaston et al., 2005; Sarris et al., 2013; Takahashi, Waters, et al., 2015; Wild et al., 2005). THEMIS satellites were close to the magnetopause, where the surface waves could penetrate and stimulate the FLRs (Chaston et al., 2005). To calculate the theoretical FLR frequency, the field line is traced using the Tsyganenko 2001 model (Tsyganenko, 2002). The mass density along the field line is obtained using the Denton et al. (2006)'s electron density model and the ion mass statistics by Takahashi et al. (2006). The Alfvén transit time

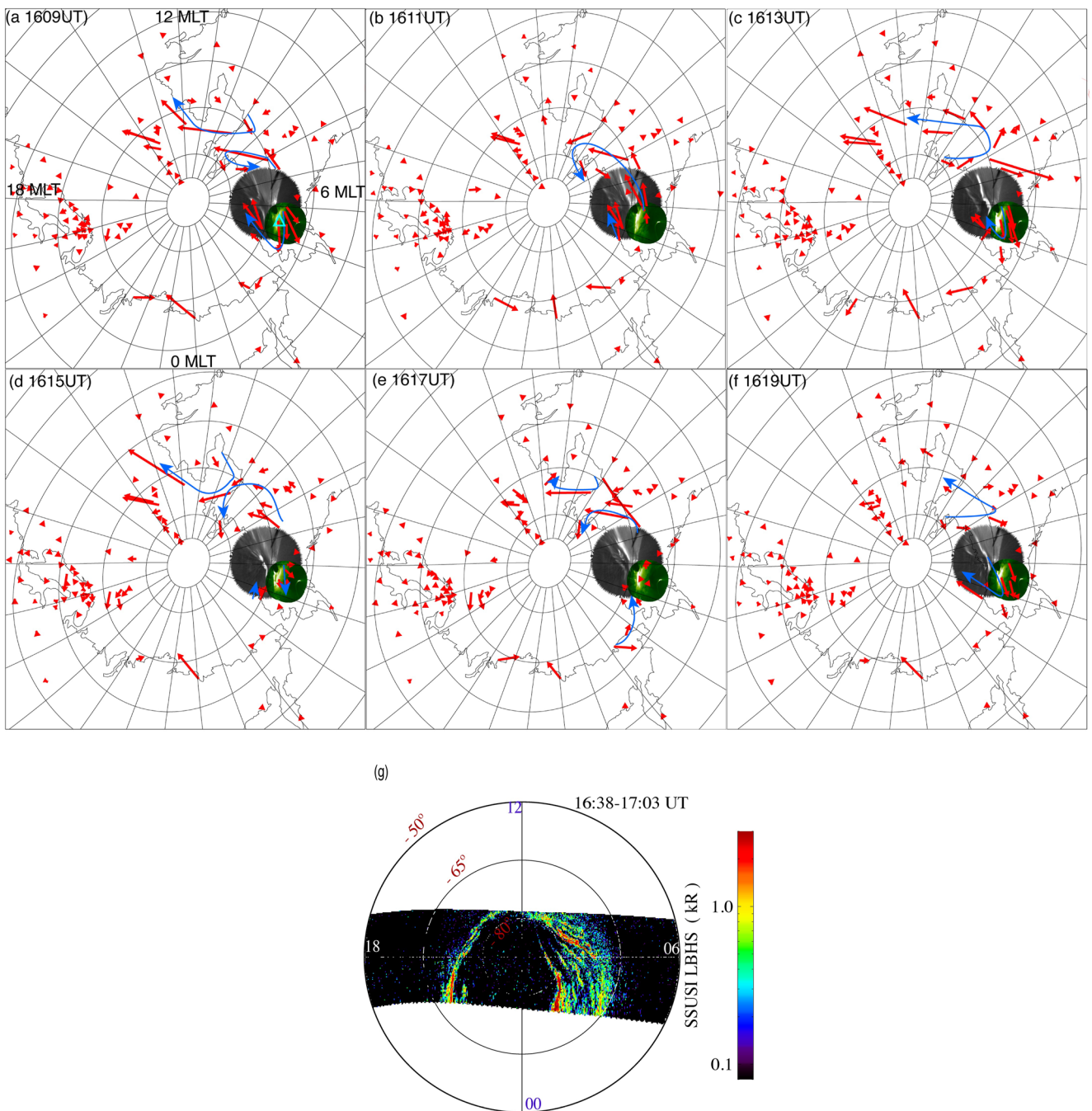


**Figure 10.** Panels (a–f) show the  $Pc5$ -filtered equivalent current and auroral distributions for the 29 December 2018 event in the same format as Figure 5. The ASIs data are from FYKN and PKR. Panel (g) is the SSUSI observations in the southern hemisphere. The light blue triangle mark the FYKN station in the first panel.

for a full bounce along the field line is calculated using these models to obtain the fundamental FLR frequency. The FLR frequency is 2.93 mHz, which is very close to the observed 3 mHz frequency. This calculation supports that the measured waves were the fundamental FLR waves.

M. O. Archer et al. (2022) stated that the oscillating parallel Poynting flux not necessarily indicate a standing Alfvén wave but a simply standing structure along the field. As suggested by Plaschke and Glassmeier (2011), Kruskal-Schwarzschild (K-S) modes show compressional signals at the magnetic equator and resemble standing Alfvén waves at high latitude. The fifth K-S mode harmonics have a frequency about 3.2 mHz (M. Archer & Plaschke, 2015). However, the magnetosheath flow speed in our cases is larger than the critical value (350 km/s),

the KH instability is unfavorable for K-S modes occurrence, and the calculated FLR frequency is closer to the observed oscillating frequency. We thus suggest that magnetopause surface waves were coupled to the standing Alfvén waves and hence the FLRs (Chen & Hasegawa, 1974; Southwood, 1974). The slow or drift mirror waves propagating tailward can be coupled to standing Alfvén waves (I. Rae et al., 2007; Walker et al., 1982), though it is difficult to discern from the observations whether Alfvén waves are followed by slow/drift mirror waves or vice versa.

## 5. Conclusions

In this paper, two Pc5 wave events observed on the dawnside on 21 November 2007 and 29 December 2018 were analyzed using space-ground conjunctions. We analyzed the Pc5 properties in the magnetosphere, magnetopause surface waves, solar wind condition, auroral structures, and the ionospheric equivalent currents. The major results are as follows:

1. The ionospheric equivalent currents were localized to the dawnside with multiple vortices of alternating polarities, forming a dawn-dusk asymmetry. The current vortices were associated with quasi-periodic poleward propagation of discrete auroral arcs. Auroral activity on the duskside was much weaker.
2. The total magnetic field and thermal pressure were anti-correlated,  $\beta$  and the drift mirror instability parameter was larger than 1. The Poynting flux was anti-sunward, and field-aligned Poynting flux oscillated around zero. The Pc5 waves of the first event propagated anti-sunward at  $\sim 400$  km/s, which was much slower than the fast-mode speed, and likely related to the anti-sunward motion of magnetopause surface waves. These observations suggest that the waves in the magnetosphere were slow or drift mirror mode waves coupling with standing Alfvén waves, and the driving source was the magnetopause surface waves.
3. Surface waves developed along the dawnside magnetopause at Pc5 frequency and were suggested to be generated by KH instability and become the source of the Pc5 waves in the magnetosphere. The solar wind observations suggests that KH instability was induced under the  $(-B_x, +B_y)$  polarity. The dawn-dusk asymmetry of Pc5 may be explained by the asymmetric occurrence of KH instability.

The unique multi-point observations in space and on the ground allowed us to reveal the Pc5 wave structure, source region, signal propagation, and a clue for the dawn-dusk asymmetry. More events are necessary to address how often ULF waves are related to KH instability, and how the surface waves are converted to magnetospheric drift mirror mode waves.

## Data Availability Statement

The THEMIS, ground magnetometer, SSUSI and Poker Flat ASI data were obtained at <http://themis.ssl.berkeley.edu/>, <https://supermag.jhuapl.edu/>, <https://ssusi.jhuapl.edu/>, and <http://optics.gi.alaska.edu/>. Date processing used SPEDAS-V3.1 (Angelopoulos et al., 2019).

## Acknowledgments

This work was supported by NASA Grant 80NSSC18K0657, 80NSSC20K0604, 80NSSC21K1683, 80NSSC20K0725, 80NSSC22K0323, 80NSSC22M0104, NAS5-02099, and 80NSSC21K1321, NSF grant AGS-1907698 and AGS-2100975, and AFOSR grant FA9559-16-1-0364. The THEMIS mission and the all-sky imagers are supported by NASA contract NAS5-02099 and Canadian Space Agency. We thank ISSI/ISSJ-BJ for the "Multi-Scale Magnetosphere-Ionosphere-Thermosphere Interaction" and "Magnetotail Dipolarizations: Archimedes Force or Ideal Collapse?" teams.

## References

- Anderson, B., Engebretson, M., Rounds, S., Zanetti, L., & Potemra, T. (1990). A statistical study of Pc 3–5 pulsations observed by the AMPTE/CCE Magnetic Fields Experiment. I. Occurrence distributions. *Journal of Geophysical Research*, 95(A7), 10495–10523. <https://doi.org/10.1029/ja095ia07p10495>
- Angelopoulos, V. (2009). The THEMIS mission. In J. L. Burch & V. Angelopoulos (Eds.), *The THEMIS mission* (pp. 5–34). Springer.
- Angelopoulos, V., Cruce, P., Drozdov, A., Grimes, E., Hatzigeorgiou, N., King, D., et al. (2019). The space physics environment data analysis system (SPEDAS). *Space Science Reviews*, 215(1), 1–46.
- Archer, M., Hartinger, M., Plaschke, F., Southwood, D., & Rastaetter, L. (2021). Magnetopause ripples going against the flow form azimuthally stationary surface waves. *Nature Communications*, 12(1), 1–14. <https://doi.org/10.1038/s41467-021-25923-7>
- Archer, M., & Plaschke, F. (2015). What frequencies of standing surface waves can the subsolar magnetopause support? *Journal of Geophysical Research: Space Physics*, 120(5), 3632–3646. <https://doi.org/10.1002/2014ja020545>
- Archer, M. O., Southwood, D. J., Hartinger, M., Rastaetter, L., & Wright, A. (2022). How a realistic magnetosphere alters the polarizations of surface, fast magnetosonic, and Alfvén waves. *Journal of Geophysical Research: Space Physics*, 127(2), e2021JA030032. <https://doi.org/10.1029/2021ja030032>
- Auster, H., Glassmeier, K., Magnes, W., Aydogar, O., Baumjohann, W., Constantinescu, D., et al. (2008). The THEMIS fluxgate magnetometer. *Space Science Reviews*, 141(1–4), 235–264. <https://doi.org/10.1007/s11214-008-9365-9>
- Baker, G. J., Donovan, E. F., & Jackel, B. J. (2003). A comprehensive survey of auroral latitude Pc5 pulsation characteristics. *Journal of Geophysical Research*, 108(A10), 1384. <https://doi.org/10.1029/2002ja009801>
- Bell, T. F. (1976). ULF wave generation through particle precipitation induced by VLF transmitters. *Journal of Geophysical Research*, 81(19), 3316–3326. <https://doi.org/10.1029/ja081i019p03316>

- Chan, A. A., Xia, M., & Chen, L. (1994). Anisotropic Alfvén-ballooning modes in Earth's magnetosphere. *Journal of Geophysical Research*, 99(A9), 17351–17366. <https://doi.org/10.1029/93ja03353>
- Chaston, C., Peticolas, L., Carlson, C., McFadden, J., Mozer, F., Wilber, M., et al. (2005). Energy deposition by Alfvén waves into the dayside auroral oval: Cluster and fast observations. *Journal of Geophysical Research*, 110(A2), A02211. <https://doi.org/10.1029/2004ja010483>
- Chen, L., & Hasegawa, A. (1974). A theory of long-period magnetic pulsations: I. Steady state excitation of field line resonance. *Journal of Geophysical Research*, 79(7), 1024–1032. <https://doi.org/10.1029/ja079i007p01024>
- Chen, L., & Hasegawa, A. (1991). Kinetic theory of geomagnetic pulsations: I. Internal excitations by energetic particles. *Journal of Geophysical Research*, 96(A2), 1503–1512. <https://doi.org/10.1029/90ja02346>
- Cheng, C., & Qian, Q. (1994). Theory of ballooning-mirror instabilities for anisotropic pressure plasmas in the magnetosphere. *Journal of Geophysical Research*, 99(A6), 11193–11209. <https://doi.org/10.1029/94ja00657>
- Claudepierre, S., Elkington, S., & Wiltberger, M. (2008). Solar wind driving of magnetospheric ULF waves: Pulsations driven by velocity shear at the magnetopause. *Journal of Geophysical Research*, 113(A5), A05218. <https://doi.org/10.1029/2007ja012890>
- Claudepierre, S., Hudson, M., Lotko, W., Lyon, J., & Denton, R. (2010). Solar wind driving of magnetospheric ULF waves: Field line resonances driven by dynamic pressure fluctuations. *Journal of Geophysical Research*, 115(A11), A11202. <https://doi.org/10.1029/2010ja015399>
- Denton, R., Takahashi, K., Galkin, I., Nsumei, P., Huang, X., Reinisch, B., et al. (2006). Distribution of density along magnetospheric field lines. *Journal of Geophysical Research*, 111(A4), A04213. <https://doi.org/10.1029/2005ja011414>
- Donovan, E., Mende, S., Jackel, B., Frey, H., Syrjäsu, M., Voronkov, I., et al. (2006). The THEMIS all-sky imaging array—System design and initial results from the prototype imager. *Journal of Atmospheric and Solar-Terrestrial Physics*, 68(13), 1472–1487. <https://doi.org/10.1016/j.jastp.2005.03.027>
- Elkington, S. R., Hudson, M. K., & Chan, A. A. (1999). Acceleration of relativistic electrons via drift-resonant interaction with toroidal-mode Pc-5 ULF oscillations. *Geophysical Research Letters*, 26(21), 3273–3276. <https://doi.org/10.1029/1999gl003659>
- Elsden, T., & Wright, A. N. (2015). The use of the Poynting vector in interpreting ULF waves in magnetospheric waveguides. *Journal of Geophysical Research: Space Physics*, 120(1), 166–186. <https://doi.org/10.1002/2014ja020748>
- Engebretson, M., Lessard, M., Bortnik, J., Green, J., Horne, R. B., Detrick, D., et al. (2008). Pc1–Pc2 waves and energetic particle precipitation during and after magnetic storms: Superposed epoch analysis and case studies. *Journal of Geophysical Research*, 113(A1), A01211. <https://doi.org/10.1029/2007ja012362>
- Fei, Y., Chan, A. A., Elkington, S. R., & Wiltberger, M. J. (2006). Radial diffusion and MHD particle simulations of relativistic electron transport by ULF waves in the September 1998 storm. *Journal of Geophysical Research*, 111(A12), A12209. <https://doi.org/10.1029/2005ja011211>
- Fujita, S., Glassmeier, K.-H., & Kamide, K. (1996). MHD waves generated by the Kelvin-Helmholtz instability in a nonuniform magnetosphere. *Journal of Geophysical Research*, 101(A12), 27317–27325. <https://doi.org/10.1029/96ja02676>
- Gillies, D. M., Knudsen, D., Rankin, R., Milan, S., & Donovan, E. (2018). A statistical survey of the 630.0-nm optical signature of periodic auroral arcs resulting from magnetospheric field line resonances. *Geophysical Research Letters*, 45(10), 4648–4655. <https://doi.org/10.1029/2018gl077491>
- Glassmeier, K.-H. (1980). Magnetometer array observations of a giant pulsation event. *Journal of Geophysics*, 48(1), 127–138.
- Glassmeier, K.-H., Othmer, C., Cramm, R., Stellmacher, M., & Engebretson, M. (1999). Magnetospheric field line resonances: A comparative planetology approach. *Surveys in Geophysics*, 20(1), 61–109. <https://doi.org/10.1023/a:1006659717963>
- Greenwald, R., & Walker, A. (1980). Energetics of long period resonant hydromagnetic waves. *Geophysical Research Letters*, 7(10), 745–748. <https://doi.org/10.1029/gl007i010p00745>
- Hao, Y., Zhao, X., Zong, Q.-G., Zhou, X.-Z., Rankin, R., Chen, X., et al. (2020). Simultaneous observations of localized and global drift resonance. *Geophysical Research Letters*, 47(17), e2020GL088019. <https://doi.org/10.1029/2020gl088019>
- Hasegawa, A. (1969). Drift mirror instability in the magnetosphere. *The Physics of Fluids*, 12(12), 2642–2650. <https://doi.org/10.1063/1.1692407>
- Hasegawa, H., Fujimoto, M., Phan, T., Reme, H., Balogh, A., Dunlop, M., et al. (2004). Rolled-up kelvin-Helmholtz vortices and associated solar wind entry at Earth's magnetopause. *Nature*, 430(7001), 755–758. <https://doi.org/10.1038/nature02799>
- Hwang, K.-J., Kuznetsova, M., Sahraoui, F., Goldstein, M., Lee, E., & Parks, G. (2011). Kelvin-Helmholtz waves under southward interplanetary magnetic field. *Journal of Geophysical Research*, 116(A8), A08210. <https://doi.org/10.1029/2011ja016596>
- Kavosi, S., & Raeder, J. (2015). Ubiquity of Kelvin-Helmholtz waves at Earth's magnetopause. *Nature Communications*, 6(1), 1–6. <https://doi.org/10.1038/ncomms8019>
- Kepko, L., & Spence, H. E. (2003). Observations of discrete, global magnetospheric oscillations directly driven by solar wind density variations. *Journal of Geophysical Research*, 108(A6), 1257. <https://doi.org/10.1029/2002ja009676>
- Kepko, L., Spence, H. E., & Singer, H. (2002). Ulf waves in the solar wind as direct drivers of magnetospheric pulsations. *Geophysical Research Letters*, 29(8), 39–1–39–4. <https://doi.org/10.1029/2001gl014405>
- Kokubun, S. (2013). ULF waves in the outer magnetosphere: Geotail observation 1 transverse waves. *Earth, Planets and Space*, 65(5), 411–433. <https://doi.org/10.5047/eps.2012.12.013>
- Li, L., Zhou, X.-Z., Zong, Q.-G., Rankin, R., Zou, H., Liu, Y., et al. (2017). Charged particle behavior in localized ultralow frequency waves: Theory and observations. *Geophysical Research Letters*, 44(12), 5900–5908. <https://doi.org/10.1002/2017gl073392>
- Li, W., Thorne, R., Bortnik, J., Nishimura, Y., & Angelopoulos, V. (2011). Modulation of whistler mode chorus waves: I. Role of compressional Pe4–5 pulsations. *Journal of Geophysical Research*, 116(A6), A06205. <https://doi.org/10.1029/2010ja016312>
- Liou, K., & Takahashi, K. (2013). Observations of field line resonance with global auroral images. *Journal of Atmospheric and Solar-Terrestrial Physics*, 105, 152–159. <https://doi.org/10.1016/j.jastp.2013.09.005>
- Liu, W., Rostoker, G., & Baker, D. (1999). Internal acceleration of relativistic electrons by large-amplitude ULF pulsations. *Journal of Geophysical Research*, 104(A8), 17391–17407. <https://doi.org/10.1029/1999ja000168>
- Liu, W., Sarris, T., Li, X., Elkington, S., Ergun, R., Angelopoulos, V., et al. (2009). Electric and magnetic field observations of Pe4 and Pe5 pulsations in the inner magnetosphere: A statistical study. *Journal of Geophysical Research*, 114(A12), A12206. <https://doi.org/10.1029/2009ja014243>
- Mann, I. R., Wright, A. N., Mills, K. J., & Nakariakov, V. M. (1999). Excitation of magnetospheric waveguide modes by magnetosheath flows. *Journal of Geophysical Research*, 104(A1), 333–353. <https://doi.org/10.1029/1998ja000026>
- McFadden, J., Carlson, C., Larson, D., Bonnell, J., Mozer, F., Angelopoulos, V., et al. (2008). Structure of plasmaspheric plumes and their participation in magnetopause reconnection: First results from THEMIS. *Geophysical Research Letters*, 35(17), L17S10. <https://doi.org/10.1029/2008gl033677>
- McHenry, M. A., Clauer, C. R., Friis-Christensen, E., Newell, P. T., & Kelly, J. (1990). Ground observations of magnetospheric boundary layer phenomena. *Journal of Geophysical Research*, 95(A9), 14995–15005. <https://doi.org/10.1029/ja095ia09p14995>
- Mende, S., Harris, S., Frey, H., Angelopoulos, V., Russell, C., Donovan, E., et al. (2009). The THEMIS array of ground-based observatories for the study of auroral substorms, *The THEMIS Mission* (pp. 357–387). [https://doi.org/10.1007/978-0-387-89820-9\\_16](https://doi.org/10.1007/978-0-387-89820-9_16)

- Motoba, T., Fujita, S., Kikuchi, T., & Tanaka, T. (2007). Solar wind dynamic pressure forced oscillation of the magnetosphere-ionosphere coupling system: A numerical simulation of directly pressure-forced geomagnetic pulsations. *Journal of Geophysical Research*, 112(A11), A11204. <https://doi.org/10.1029/2006ja012193>
- Motoba, T., Kikuchi, T., Okuzawa, T., & Yumoto, K. (2003). Dynamical response of the magnetosphere-ionosphere system to a solar wind dynamic pressure oscillation. *Journal of Geophysical Research*, 108(A5), 1206. <https://doi.org/10.1029/2002ja009696>
- Motoba, T., Ogawa, Y., Ebihara, Y., Kadokura, A., Gerrard, A., & Weatherwax, A. (2021). Daytime Pc5 diffuse auroral pulsations and their association with outer magnetospheric ULF waves. *Journal of Geophysical Research: Space Physics*, 126(8), e2021JA029218. <https://doi.org/10.1029/2021ja029218>
- Nambu, M., Tamao, T., Miura, A., Taniguchi, H., Bujarbarua, S., & Sarma, S. (1986). Theory of ULF-modulated electrostatic wave. *Planetary and Space Science*, 34(9), 845–849. [https://doi.org/10.1016/0032-0633\(86\)90082-6](https://doi.org/10.1016/0032-0633(86)90082-6)
- Nishimura, Y., Bortnik, J., Li, W., Thorne, R., Ni, B., Lyons, L., et al. (2013). Structures of dayside whistler-mode waves deduced from conjugate diffuse aurora. *Journal of Geophysical Research: Space Physics*, 118(2), 664–673. <https://doi.org/10.1029/2012ja018242>
- Nosé, M., Iyemori, T., Sugiura, M., & Slavin, J. (1995). A strong dawn/dusk asymmetry in Pc5 pulsation occurrence observed by the DE-1 satellite. *Geophysical Research Letters*, 22(15), 2053–2056. <https://doi.org/10.1029/95gl01794>
- Nowada, M., Shue, J.-H., Lin, C.-H., Sakurai, T., Sibeck, D., Angelopoulos, V., et al. (2009). Alfvénic plasma velocity variations observed at the inner edge of the low-latitude boundary layer induced by the magnetosheath mirror mode waves: A THEMIS observation. *Journal of Geophysical Research*, 114(A7), A07208. <https://doi.org/10.1029/2008ja014033>
- Nykyri, K. (2013). Impact of MHD shock physics on magnetosheath asymmetry and Kelvin-Helmholtz instability. *Journal of Geophysical Research: Space Physics*, 118(8), 5068–5081. <https://doi.org/10.1002/jgra.50499>
- Nykyri, K., Johnson, J., Kronberg, E., Turner, D., Wing, S., Cohen, I., et al. (2021). Magnetospheric multiscale observations of the source region of energetic electron microinjections along the duskside, high-latitude magnetopause boundary layer. *Geophysical Research Letters*, 48(9), e2021GL092466. <https://doi.org/10.1029/2021gl092466>
- Paxton, L. J., Morrison, D., Zhang, Y., Kil, H., Wolven, B., Ogorzalek, B. S., et al. (2002). Validation of remote sensing products produced by the Special Sensor Ultraviolet Scanning Imager (SSUSI): A far UV-imaging spectrograph on DMSP F-16. In *Optical spectroscopic techniques, remote sensing, and instrumentation for atmospheric and space research IV* (Vol. 4485, pp. 338–348).
- Plaschke, F., & Glassmeier, K.-H. (2011). Properties of standing Kruskal-Schwarzschild-modes at the magnetopause. In *Annales geophysicae* (Vol. 29, pp. 1793–1807).
- Pu, Z.-Y., & Kivelson, M. G. (1983). Kelvin-Helmholtz instability at the magnetopause: Solution for compressible plasmas. *Journal of Geophysical Research*, 88(A2), 841–852. <https://doi.org/10.1029/ja088ia02p00841>
- Pulkkinen, A., Bernabeu, E., Thomson, A., Viljanen, A., Pirjola, R., Boteler, D., et al. (2017). Geomagnetically induced currents: Science, engineering, and applications readiness. *Space Weather*, 15(7), 828–856. <https://doi.org/10.1002/2016sw001501>
- Rae, I., Donovan, E., Mann, I., Fenrich, F., Watt, C., Milling, D., et al. (2005). Evolution and characteristics of global Pc5 ULF waves during a high solar wind speed interval. *Journal of Geophysical Research*, 110(A12), A12211. <https://doi.org/10.1029/2005ja011007>
- Rae, I., Mann, I., Dent, Z., Milling, D., Donovan, E., & Spanswick, E. (2007). Multiple field line resonances: Optical, magnetic and absorption signatures. *Planetary and Space Science*, 55(6), 701–713. <https://doi.org/10.1016/j.pss.2006.02.009>
- Rae, I. J., Mann, I. R., Watt, C. E., Kistler, L. M., & Baumjohann, W. (2007). Equator-S observations of drift mirror mode waves in the dawnside magnetosphere. *Journal of Geophysical Research*, 112(A11), A11203. <https://doi.org/10.1029/2006ja012064>
- Ren, J., Zong, Q., Zhou, X., Rankin, R., Wang, Y., Gu, S., & Zhu, Y. (2017). Phase relationship between ULF waves and drift-bounce resonant ions: A statistical study. *Journal of Geophysical Research: Space Physics*, 122(7), 7087–7096. <https://doi.org/10.1002/2016ja023848>
- Ren, J., Zong, Q.-G., Miyoshi, Y., Zhou, X., Wang, Y., Rankin, R., et al. (2017). Low-energy (<200 eV) electron acceleration by ULF waves in the plasmaspheric boundary layer: Van Allen Probes observation. *Journal of Geophysical Research: Space Physics*, 122(10), 9969–9982. <https://doi.org/10.1002/2017ja024316>
- Ren, J., Zong, Q.-G., Zhou, X., Rankin, R., & Wang, Y. (2016). Interaction of ULF waves with different ion species: Pitch angle and phase space density implications. *Journal of Geophysical Research: Space Physics*, 121(10), 9459–9472. <https://doi.org/10.1002/2016ja022995>
- Rostoker, G., Skone, S., & Baker, D. N. (1998). On the origin of relativistic electrons in the magnetosphere associated with some geomagnetic storms. *Geophysical Research Letters*, 25(19), 3701–3704. <https://doi.org/10.1029/98gl02801>
- Russell, C., Chi, P., Dearborn, D., Ge, Y., Kuo-Tiong, B., Means, J., et al. (2008). THEMIS ground-based magnetometers. *Space Science Reviews*, 141(1), 389–412. <https://doi.org/10.1007/s11214-008-9337-0>
- Samson, J., Harrold, B., Ruohoniemi, J., Greenwald, R., & Walker, A. (1992). Field line resonances associated with MHD waveguides in the magnetosphere. *Geophysical Research Letters*, 19(5), 441–444. <https://doi.org/10.1029/92gl00116>
- Sarris, T., Li, X., Liu, W., Argyriadis, E., Boudouridis, A., & Ergun, R. (2013). Mode number calculations of ULF field-line resonances using ground magnetometers and THEMIS measurements. *Journal of Geophysical Research: Space Physics*, 118(11), 6986–6997. <https://doi.org/10.1002/2012ja018307>
- Sarris, T., Li, X., & Singer, H. (2009). A long-duration narrowband Pc5 pulsation. *Journal of Geophysical Research*, 114(A1), A01213. <https://doi.org/10.1029/2007ja012660>
- Shen, X.-C., Shi, Q., Wang, B., Zhang, H., Hudson, M. K., Nishimura, Y., et al. (2018). Dayside magnetospheric and ionospheric responses to a foreshock transient on 25 June 2008: 1. FLR observed by satellite and ground-based magnetometers. *Journal of Geophysical Research: Space Physics*, 123(8), 6335–6346. <https://doi.org/10.1029/2018ja025349>
- Shi, X., Hartinger, M. D., Baker, J., Ruohoniemi, J. M., Lin, D., Xu, Z., et al. (2020). Multipoint conjugate observations of dayside ULF waves during an extended period of radial IMF. *Journal of Geophysical Research: Space Physics*, 125(11), e2020JA028364. <https://doi.org/10.1029/2020ja028364>
- Shi, X., Ruohoniemi, J., Baker, J., Lin, D., Bland, E., Hartinger, M., & Scales, W. (2018). Survey of ionospheric Pc3-5 ULF wave signatures in Super-DARN high time resolution data. *Journal of Geophysical Research: Space Physics*, 123(5), 4215–4231. <https://doi.org/10.1029/2017ja025033>
- Soto-Chavez, A., Lanzerotti, L., Manweiler, J., Gerrard, A., Cohen, R., Xia, Z., et al. (2019). Observational evidence of the drift-mirror plasma instability in Earth's inner magnetosphere. *Physics of Plasmas*, 26(4), 042110. <https://doi.org/10.1063/1.5083629>
- Southwood, D. (1974). Some features of field line resonances in the magnetosphere. *Planetary and Space Science*, 22(3), 483–491. [https://doi.org/10.1016/0032-0633\(74\)90078-6](https://doi.org/10.1016/0032-0633(74)90078-6)
- Southwood, D. (1976). A general approach to low-frequency instability in the ring current plasma. *Journal of Geophysical Research*, 81(19), 3340–3348. <https://doi.org/10.1029/ja081i019p03340>
- Takahashi, K., Denton, R. E., Anderson, R. R., & Hughes, W. J. (2006). Mass density inferred from toroidal wave frequencies and its comparison to electron density. *Journal of Geophysical Research*, 111(A1), A01201. <https://doi.org/10.1029/2005ja011286>

- Takahashi, K., Hartinger, M. D., Angelopoulos, V., & Glassmeier, K.-H. (2015). A statistical study of fundamental toroidal mode standing Alfvén waves using THEMIS ion bulk velocity data. *Journal of Geophysical Research: Space Physics*, 120(8), 6474–6495. <https://doi.org/10.1002/2015ja021207>
- Takahashi, K., & Ukhorskiy, A. Y. (2008). Timing analysis of the relationship between solar wind parameters and geosynchronous Pc5 amplitude. *Journal of Geophysical Research*, 113(A12), A12204. <https://doi.org/10.1029/2008ja013327>
- Takahashi, K., Waters, C., Glassmeier, K.-H., Kletzing, C. A., Kurth, W. S., & Smith, C. W. (2015). Multifrequency compressional magnetic field oscillations and their relation to multiharmonic toroidal mode standing Alfvén waves. *Journal of Geophysical Research: Space Physics*, 120(12), 10–384. <https://doi.org/10.1002/2015ja021780>
- Tang, B., Wang, C., & Li, W. (2013). The magnetosphere under the radial interplanetary magnetic field: A numerical study. *Journal of Geophysical Research: Space Physics*, 118(12), 7674–7682. <https://doi.org/10.1002/2013ja019155>
- Tsyganenko, N. (2002). A model of the near magnetosphere with a dawn-dusk asymmetry 1. Mathematical structure. *Journal of Geophysical Research*, 107(A8), SMP 12-1–SMP 12-15. <https://doi.org/10.1029/2001ja000219>
- Vennnerström, S. (1999). Dayside magnetic ULF power at high latitudes: A possible long-term proxy for the solar wind velocity? *Journal of Geophysical Research*, 104(A5), 10145–10157. <https://doi.org/10.1029/1999ja900015>
- Vidal-Luengo, S., & Moldwin, M. B. (2021). Global magnetosphere response to solar wind dynamic pressure pulses during northward IMF using the heliophysics system observatory. *Journal of Geophysical Research: Space Physics*, 126(2), e2020JA028587. <https://doi.org/10.1029/2020ja028587>
- Walker, A. (1981). The Kelvin-Helmholtz instability in the low-latitude boundary layer. *Planetary and Space Science*, 29(10), 1119–1133. [https://doi.org/10.1016/0032-0633\(81\)90011-8](https://doi.org/10.1016/0032-0633(81)90011-8)
- Walker, A., Greenwald, R., Korth, A., & Kremser, G. (1982). STARE and GEOS 2 observations of a storm time Pc 5 ULF pulsation. *Journal of Geophysical Research*, 87(A11), 9135–9146. <https://doi.org/10.1029/ja087ia11p09135>
- Wang, B., Nishimura, Y., Hartinger, M., Sivadas, N., Lyons, L. L., Varney, R. H., & Angelopoulos, V. (2020). Ionospheric modulation by storm time Pc5 ULF pulsations and the structure detected by PFISR-THEMIS conjunction. *Geophysical Research Letters*, 47(16), e2020GL089060. <https://doi.org/10.1029/2020gl089060>
- Wild, J. A., Yeoman, T., & Waters, C. (2005). Revised time-of-flight calculations for high-latitude geomagnetic pulsations using a realistic magnetospheric magnetic field model. *Journal of Geophysical Research*, 110(A11), A11206. <https://doi.org/10.1029/2004ja010964>
- Yagova, N. V., Pilipenko, V. A., Sakharov, Y. A., & Selivanov, V. N. (2021). Spatial scale of geomagnetic Pc5/Pi3 pulsations as a factor of their efficiency in generation of geomagnetically induced currents. *Earth, Planets and Space*, 73(1), 88. <https://doi.org/10.1186/s40623-021-01407-2>
- Zhang, X., Zong, Q.-G., Wang, Y., Zhang, H., Xie, L., Fu, S., et al. (2010). ULF waves excited by negative/positive solar wind dynamic pressure impulses at geosynchronous orbit. *Journal of Geophysical Research*, 115(A10), A10221. <https://doi.org/10.1029/2009ja015016>
- Zhao, X., Hao, Y., Zong, Q.-G., Zhou, X.-Z., Yue, C., Chen, X., et al. (2020). Origin of electron boomerang stripes: Localized ULF wave-particle interactions. *Geophysical Research Letters*, 47(17), e2020GL087960. <https://doi.org/10.1029/2020gl087960>
- Zhu, X., & Kivelson, M. G. (1994). Compressional ULF waves in the outer magnetosphere: 2. A case study of Pc 5 type wave activity. *Journal of Geophysical Research*, 99(A1), 241–252. <https://doi.org/10.1029/93ja02106>
- Zong, Q., Rankin, R., & Zhou, X. (2017). The interaction of ultra-low-frequency Pc3–5 waves with charged particles in Earth's magnetosphere. *Reviews of Modern Plasma Physics*, 1(1), 1–90. <https://doi.org/10.1007/s41614-017-0011-4>